

Optical conductivity of the t_{2g} two-dimensional electron gas

Ming Xie,¹ Guru Khalsa,¹ and A.H. MacDonald¹

¹*Department of Physics, University of Texas at Austin, Austin TX 78712-1081, USA*

(Dated: February 27, 2024)

Motivated by recent interest in perovskite surfaces and heterostructures, we present an analysis of the Kubo conductivity of a two-dimensional electron gas (2DEG) formed in the t_{2g} bands of an oxide with perovskite structure. We find that when the electric field is polarized in the plane of the 2DEG, the optical conductivity is dominated by nearly independent Drude contributions from two-dimensional subband Fermi surfaces, whereas for perpendicular-to-plane polarization it has strong intersubband features. Our analysis suggests that perpendicular-to-plane optical conductivity studies may help advance understanding of the interplay between lattice distortions and electron-electron interactions in complex oxide 2DEG quantum confinement physics.

PACS numbers: 78.68.+m, 73.20.-r, 68.47.Gh, 73.40.-c

I. INTRODUCTION

Heterostructures and multilayers based on the perovskite lattice have recently been the focus of an enormous research effort. The perovskite lattice supports much of the periodic table¹ and can be grown epitaxially with very high quality.² Perovskite heterointerfaces often have properties that are drastically distinct from those of their parent bulk materials. The most well known example of this tendency is the polar/non-polar interface³ between the band insulators LaAlO_3 and SrTiO_3 which hosts a high mobility two-dimensional electron gas (2DEG) formed mainly from the t_{2g} orbitals of SrTiO_3 that can be magnetic⁴ or superconducting⁵ or both.⁶ There have by now been many studies of SrTiO_3 t_{2g} 2DEGs formed at various interfaces and surfaces.^{7–11} 2DEGs that are mostly similar in character but have much stronger spin-orbit (SO) coupling can be formed at KTaO_3 interfaces and surfaces.^{12,13} In both SrTiO_3 and KTaO_3 , it has been shown that because of strong and non-linear dielectric response at low temperature, the 2DEGs consist of a high electron density component containing mostly electrons that are strongly confined to the surface or interface, and a low-density tail component consisting of weakly confined electrons that occupy closely spaced subbands which extend $\sim 10\text{-}20$ nm into the bulk of the material.^{14,15}

Optical studies have played an important role in conventional semiconductor 2DEGs.^{16,17} Absorption of light with electric fields polarized perpendicular to the 2DEG plane has been especially valuable because it measures intersubband optical transition energies and in this way characterizes 2DEG quantum confinement. No intersubband optical response is observed¹⁸ when light is polarized with its electric field in the 2DEG plane. Because optical spectra can probe intersubband transition energies, optical characterization also has the potential to play an important role in sorting out the quantum confinement physics in t_{2g} 2DEGs. Experimental guidance would be especially valuable because of the complicating influence in the oxide case by non-linear dielectric

screening and the greater likelihood of structural distortions and defects at interfaces. In this article we explore the optical conductivity of t_{2g} 2DEGs theoretically, with a view toward shedding light on the information which can be garnered from future experimental studies.¹⁹ We find that the optical response of the t_{2g} 2DEG is dominated by electrons within the first few layers of the surface or interface. When light is polarized in the 2D plane, the conductivity is dominated by a Drude peak to which all occupied t_{2g} orbitals contribute. The integrated strength of this peak provides information on the carrier density which is complementary to that available from Hall effect measurements. There are however weak intersubband peaks which could be very revealing if they could be detected. Measurements of the peak frequencies should be very valuable in constraining confinement models. The corresponding peak strengths are sensitive to hybridization between different t_{2g} orbitals, which is weak in the ideal case, and may therefore shed light on spin-orbit coupling strengths and on structural distortions of the pseudocubic cell near the interface. For light polarized perpendicular-to-plane, the optical conductivity has large intersubband features related to hopping amplitudes perpendicular to the interface, and to the confining potential. In Sections II and III below we briefly discuss the model we use for a t_{2g} 2DEG and comment on the Kubo formula expressions we use for the conductivity. Our main results are presented and discussed in Section IV. The paper concludes in Section V with a brief summary and conclusions.

II. MODEL

In the perovskite ABO_3 unit cell, the B cation is surrounded by an octahedral oxygen cage which lifts its d-orbital degeneracy, pushing the $e_g = \{x^2 - y^2, 3z^2\}$ levels up relative to the $t_{2g} = \{yz, zx, xy\}$ levels. We focus on systems with conduction bands that have t_{2g} character and are well separated from oxygen p-orbital derived valance bands. In a cubic environment, the yz , zx , and xy members of the t_{2g} manifold are very weakly

hybridized. Under most circumstances atomic-like SO coupling is the dominant source of hybridization. When it is neglected, the three bands therefore contribute essentially independently to physical properties of 2DEG, which we assume form in $x - y$ planes. The symmetries which lead to this circumstance can be understood by considering a two-center approximation description in which an xy electron hops along the x -direction within a BO_2 plane from a B atom xy orbital to another B atom via π bonding to the p_y orbital of the intermediate oxygen atom that is virtually occupied. We define this and other symmetry equivalent metal to metal effective hopping amplitudes as $-t$. For hopping in the y -direction, the B atom xy orbital hops through an oxygen p_x orbital to a neighboring B atom xy orbital with the same effective hopping amplitude. There is also a smaller but still important z -direction hopping amplitude $-t'$ for xy orbitals which connects one BO_2 layer to another that is closer to or further from the interface. $\{yz, zx\}$ orbitals, on the other hand, have strong $(-t)$ out-of-plane hopping and weak hopping $(-t')$ in one of two in-plane directions. These orbital conserving hopping processes are responsible for most of the qualitative properties of t_{2g} 2DEGs and are readily expressed mathematically by the system's tight binding model Hamiltonian.

For a single BO_2 layer, the tight-binding Hamiltonian within the t_{2g} subspace is,

$$H_{SL} = \sum_{\vec{k}, \gamma, \sigma} \epsilon_\gamma(\vec{k}) \hat{n}_{\vec{k}, \gamma, \sigma} \quad (1)$$

where \vec{k} is the in-plane crystal momentum, $\gamma = \{yz, zx, xy\}$, and σ is the spin index. The $\epsilon_\gamma(\vec{k})$ are defined by,

$$\begin{aligned} \epsilon_{yz}(\vec{k}) &= -2t' \cos(k_x a) - 2t \cos(k_y a) \\ \epsilon_{zx}(\vec{k}) &= -2t \cos(k_x a) - 2t' \cos(k_y a) \\ \epsilon_{xy}(\vec{k}) &= -2t \cos(k_x a) - 2t \cos(k_y a) \end{aligned} \quad (2)$$

Similarly the interlayer tunneling Hamiltonian is,

$$H_{inter} = - \sum_{\langle l, l' \rangle, \gamma, \sigma} t_\gamma \hat{c}_{\vec{k}, l, \gamma, \sigma}^\dagger \hat{c}_{\vec{k}, l', \gamma, \sigma}, \quad (3)$$

where $\langle l, l' \rangle$ are neighboring layers, $t_\gamma = t'$ for $\gamma = xy$, and $t_\gamma = t$ for $\gamma = \{yz, zx\}$. Spin-orbit coupling of the cation d -orbitals is mainly atomic in character. In the calculations described below we have used a model¹⁴ in which we project atomic spin-orbit coupling onto the t_{2g} space. Note that, although this model contains spin-orbit coupling, it does not capture the processes which can lead to Rashba¹³ spin-orbit induced momentum-splitting of the Bloch band's double spin degeneracy.

Most t_{2g} 2DEGs are formed near the surface of a sample sitting on a grounded substrate. It follows that the electric field goes to zero below the 2DEG and that the

electric field above the 2DEG is proportional to the electron density. The electric field in the region occupied by the 2DEG is screened both by the 2DEG electrons and by distortions of the ionic host lattice. The extremely large dielectric constant of the host material is related to its soft anharmonic optical phonon modes, which are in turn related to the material's nascent ferroelectricity. We have previously described¹⁴ a simple model which accounts for this complex physical situation qualitatively. We employ that model for the illustrative optical conductivity calculations that we report on below, forcing the 2DEG to lie entirely within the first 60 BO_2 layers. Because t_{2g} 2DEGs can be prepared over a very wide density regime, we have considered three representative areal densities n - referred to below as "low" ($n = 2.3 \times 10^{13} \text{ cm}^{-2}$), "medium" ($n = 2. \times 10^{14} \text{ cm}^{-2}$), and "high" ($n = 5.9 \times 10^{14} \text{ cm}^{-2}$) (as described in Ref. 14). The present calculations are motivated by the expectation that quantitative comparisons between experiment and this simple theoretical model can be used to refine approximations and improve its predictive power.

III. LINEAR RESPONSE THEORY

We consider the response of the 2DEG current to a weak external electromagnetic field. In the random phase approximation, the conductivity tensor is given by the well-known Kubo formula:²⁰

$$\sigma_{\alpha\beta}(\omega) = i\hbar \sum_{m, n, \vec{k}} \left(\frac{f_n - f_m}{\epsilon_m - \epsilon_n} \right) \frac{\langle m, \vec{k} | \hat{j}_\alpha | n, \vec{k} \rangle \langle n, \vec{k} | \hat{j}_\beta | m, \vec{k} \rangle}{\hbar\omega - (\epsilon_m - \epsilon_n) + i\eta} \quad (4)$$

where m, n are band and α, β Cartesian direction indices, \vec{k} is the 2DEG crystal momentum, and \hat{j}_α is the paramagnetic component of the current operator for which an explicit expression is given below. The dependence of the Fermi distribution function f_n and the band energy ϵ_n on \vec{k} is left implicit for notational simplicity. The ratio of Fermi factor to energy differences should be understood as a derivative in the $m = n$ limit so that the intraband contribution to the conductivity is

$$\sigma_{\alpha\beta}^{IB}(\omega) = i\hbar \sum_{n, \vec{k}} \left(-\frac{\partial f}{\partial \epsilon} \right) \frac{\langle n, \vec{k} | \hat{j}_\alpha | n, \vec{k} \rangle \langle n, \vec{k} | \hat{j}_\beta | n, \vec{k} \rangle}{\hbar\omega + i\eta} \quad (5)$$

We treat $\eta = \hbar\tau^{-1}$ as a phenomenological parameter which accounts for the Bloch state lifetimes, assigning it a value that is independent of band index.

In Eq. (4) we have taken the limit $q \rightarrow 0$ because wavelengths are long compared to lattice constants in the optical frequency regime. The paramagnetic current operator²¹ is therefore given by the commutator of the Hamiltonian with the polarization operator \hat{P} :

$$\hat{j}_\alpha = -\frac{ie}{\hbar} [H, \hat{P}_\alpha] \quad (6)$$

In the tight binding approximation, electrons are considered to sit on lattice sites so position is discrete in real space. The polarization operator therefore takes the form: $\hat{P} = \sum_i R_i \hat{n}_i$. It follows that the in-plane current operator is given by taking the derivative of the Hamiltonian with respect to crystal momentum. Therefore only

$$j_x = \frac{e}{\hbar} \frac{\partial H}{\partial k_x} = \frac{ea}{\hbar} \begin{pmatrix} -2t' \sin(k_x a) & 0 & 0 \\ 0 & -2t \sin(k_x a) & 0 \\ 0 & 0 & -2t \sin(k_x a) \end{pmatrix}. \quad (7)$$

Note that the in-plane current operator couples only subbands with the same orbital character and that its action is independent of position relative to the interface. In the absence of orbital hybridization (due to SO coupling in the model we considered) the bare Hamiltonian is also diagonal in orbital. It follows that in this case there are no intersubband transition contributions to the in-plane conductivity, either from transitions between subbands with the same orbital character or from transitions between subbands with different orbital character. When hybridization is neglected the in-plane orbital conductivity has only a Drude response centered on $\omega \rightarrow 0$.

Because the system is finite in the z-direction, the commutator in Eq. 6 is best evaluated in position space for this current component. We find that

$$j_z = -\frac{ie}{\hbar} \sum_{\vec{k}, l, \gamma} at_\gamma \left(\hat{c}_{\vec{k}, l+1, \gamma}^\dagger \hat{c}_{\vec{k}, l, \gamma} - \hat{c}_{\vec{k}, l-1, \gamma}^\dagger \hat{c}_{\vec{k}, l, \gamma} \right) \quad (8)$$

where $t_\gamma = \{t, t'\}$ for hopping the z-direction in the $\{yz, zx, xy\}$ basis. Because j_z is off-diagonal in layer index, optical transitions between different subbands with the same orbital character are allowed even in the absence of inter-orbital hybridization. Although orbital hybridization can weakly allow additional optical transitions, intra-orbital contributions dominate the perpendicular-to-plane optical response, especially so when the Fermi energy is much larger than the SO splitting. For the calculations presented below this criterion is satisfied at medium and high densities.

The real part of the longitudinal conductivity tensor satisfies certain sum rules which are useful for verifying numerical results and also potentially useful in interpreting experiments. These sum rules limit conductivity contributions from intersubband transitions. By employing the commutation relation (6), we obtain the following sum rules for in-plane and perpendicular-to-plane con-

ductivity tensors:

$$\int_{-\infty}^{\infty} d\omega \text{Re}[\sigma_{xx}(\omega)] = \frac{\pi e^2}{\hbar^2} \sum_{m, \vec{k}} \langle m\vec{k} | \frac{\partial^2 H}{\partial k_x^2} | m\vec{k} \rangle f_m \\ = \pi e^2 \sum_n \frac{n_n}{m_{xx,n}^*}, \quad (9)$$

$$\int_{-\infty}^{\infty} d\omega \text{Re}[\sigma_{zz}(\omega)] = -\frac{i\pi e}{\hbar} \sum_{m, \vec{k}} \langle m\vec{k} | [\hat{j}_z, \hat{P}_z] | m\vec{k} \rangle f_m, \quad (10)$$

Eq. 9 is the standard result that the electronic contribution to optical conductivity integrated over all frequency is proportional to the density of electrons in that band scaled by the inverse effective mass. The second form of the right hand side of Eq. 9 applies only in the low density limit in which the parabolic approximation for the band dispersion relations is accurate. Here n_n corresponds to the density of the n^{th} band. In the absence of SO coupling, Eq. 9 may be simplified further to,

$$\frac{\pi e^2}{\hbar^2} \sum_{\gamma} \frac{t_\gamma a^2}{2} n_\gamma, \quad (11)$$

where n_γ is the total density associated with electrons of orbital character γ . The commutator in Eq. 10 is:

$$-\frac{ia^2}{\hbar} \sum_{\vec{k}, l, \gamma} t_\gamma (\hat{c}_{\vec{k}, l+1, \gamma}^\dagger \hat{c}_{\vec{k}, l, \gamma} + \hat{c}_{\vec{k}, l-1, \gamma}^\dagger \hat{c}_{\vec{k}, l, \gamma}). \quad (12)$$

Contributions to Eq. 10 are therefore directly proportional to the amplitude for an electron in layer l to hop to a neighboring layer, $l \pm 1$.

IV. RESULT AND DISCUSSION

Fig. 1 shows the real part of the in-plane optical conductivity for $\hbar\omega$ up to 200meV, including both the Drude

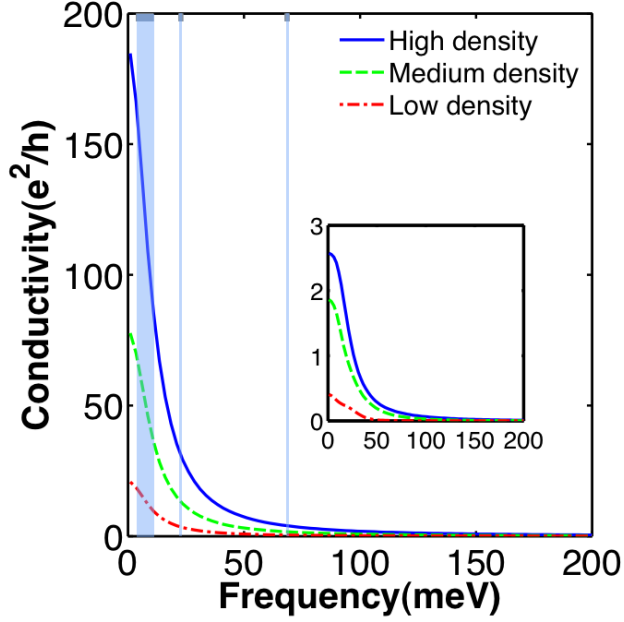


FIG. 1: (Color online) In-plane optical conductivity of a SrTiO₃ 2DEG in e^2/h units for light polarized in the plane of the t_{2g} 2DEG at high ($5.9 \times 10^{-14} \text{ cm}^{-2}$), medium ($2 \times 10^{-14} \text{ cm}^{-2}$), and low ($2.3 \times 10^{-13} \text{ cm}^{-2}$) carrier densities as defined in Ref. 14. The shaded region in the figure highlights the frequency region in which the electronic conductivity is expected to be obscured by optical phonons. η has been set to 10 meV in order to yield $\omega \rightarrow 0$ limits that are similar to those observed experimentally. The inset shows the intersubband contribution to the conductivity which is contributed mainly by electrons in the low-density tail.

conductivity and the intersubband part of the conductivity with the phenomenological scattering rate taken to be the same for both ($\eta = 10 \text{ meV}$). This value of η yields Drude peak heights in the range typical of recent *dc* resistivity measurements.²² The Drude conductivity increases monotonically with the density of the 2DEG as expected from the sum rules discussed above. The in-plane optical conductivity is dominated by the Drude part for all densities. The integrated Drude weight may be used to estimate the total density, provided the effective masses in Eq. 11 can be estimated. From Eq. 2 the xy and xz bands masses along the x -direction are larger than the yz mass (by a factor ~ 10). This suggests, that in this limit, the Drude weight will typically be dominated by the xy and xz pockets. The Hall conductivity can be used to provide a complementary estimate of the total carrier density which weights individual orbitals differently.²³ Measurements of both quantities could be very helpful in obtaining reliable experimental carrier density estimates.

As shown in the inset in Fig.1 there is a small intersubband contribution to the conductivity which originates from the low-density tail states. For these states, subband separations are comparable to spin-orbit coupling strengths ($\Delta_{SO} = 18 \text{ meV}$) allowing for considerable or-

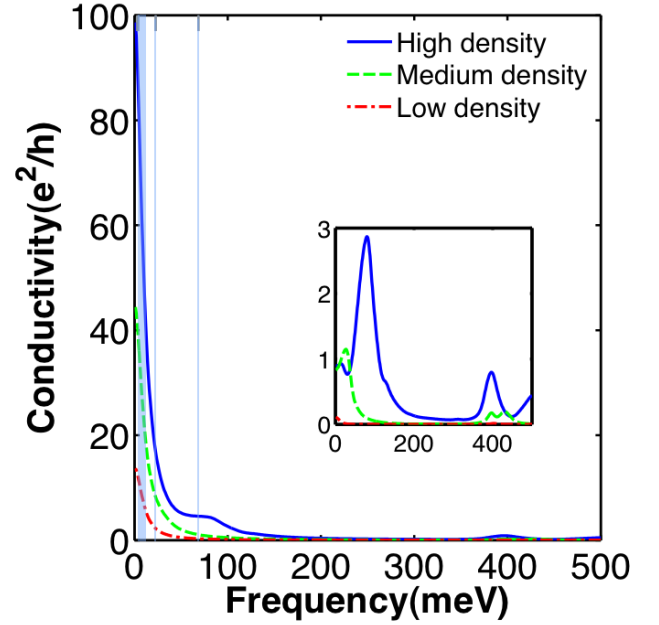


FIG. 2: (Color online) In-plane optical conductivity of a t_{2g} 2DEG with strong atomic spin-orbit coupling with strength $\Delta_{SO} = 400 \text{ meV}$. The inset plots the intersubband part only. η has been set to 10 meV .

bital hybridization. The intersubband contribution will likely be difficult to isolate experimentally because it is weak in a relative sense. Additionally because of the small band separations of tail states it will be difficult to separate spectrally from the Drude peak at typical values of η because it is also peaked close to $\omega = 0$. Intersubband features might be observable in systems with spin-orbit coupling strengths that are larger than those of SrTiO₃ ($\Delta_{SO} = 18 \text{ meV}$) or in systems with substantially smaller lifetime broadening than is currently achievable (see below).

We remark that the utility of optical conductivity measurements as a probe of electronic properties is mitigated by the presence of strong optical phonon contributions. In Fig. 1 we have shaded the frequency ranges expected²⁴ to be obscured by the three optical phonon modes which overlap with 2DEG energy scales. The frequency of the low energy phonon at the $\vec{q} = 0$ is strongly dependent on temperature. To represent this we have included a shaded region spanning its temperature dependence.

In t_{2g} 2DEG systems with strong spin-orbit coupling, spectral features associated with transitions between strongly confined orbitals may become visible. To illustrate this effect, we have artificially set the atomic spin-orbit coupling strength parameter $\Delta_{SO} \rightarrow 400 \text{ meV}$ in the SrTiO₃ 2DEG model and repeated the in-plane optical response calculation. In Fig. 2 we see that transitions within the weakly-confined subbands are again obscured because of the Bloch state lifetime. Now, however, the spin-orbit coupling strength is strong enough to induce appreciable hybridization of the strongly-confined sub-

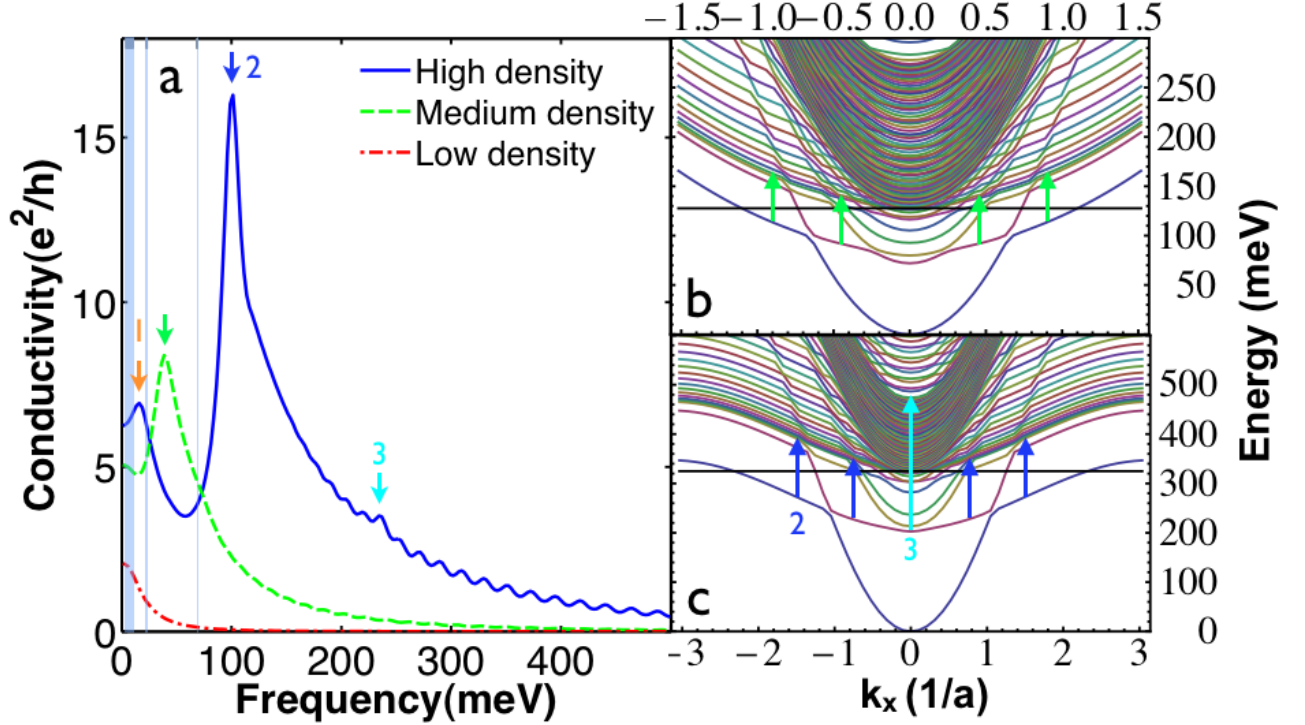


FIG. 3: (Color online) Perpendicular-to-plane optical conductivities for low medium and high densities (a). (b) Self-consistent band structure for a density of $2 \times 10^{14} \text{cm}^{-2}$. (c) Self-consistent 2DEG subband structure for a density of $5.9 \times 10^{14} \text{cm}^{-2}$. The main optical transitions for perpendicular-to-plane polarization are indicated by color coordinated arrows the conductivity and bandstructure plots. Feature 1 is at too low a frequency to be evident in on the energy scale of c. The disorder-broadening η has been set to 10meV.

bands. The inset of Fig. 2 again shows the intersubband optical response features are most prominent at high carrier densities. The strongest feature is a broad peak centered at ~ 400 meV associated with transitions to bulk spin-orbit split bands near the bottom of the conduction band. It is present at all carrier densities, but stronger at higher carrier densities. A second feature associated with the confinement energy scale is now allowed because of orbital hybridization within the t_{2g} manifold. Even in the high density case, the 400 meV SO coupling is larger than the confinement energy of the lowest subband. This suggests that all bands have strongly hybridized t_{2g} character. Since the SO coupling is local, it does not contribute to the current operator. Therefore, the matrix elements of the current operator in the optical conductivity still favor xy and zx orbitals due to their strong bonding in the x -direction. The peak at ~ 80 meV is dominated by a peak in the zx projected density of states related to the confinement energy of the most confined $\{yz, zx\}$ bands. Because the energy scales associated with structural deformations (of the parent material or induced by the interface) are not expected to be this large,²⁵ we conclude that in the absence of large SO coupling in plane conductivity measurements are unlikely to provide useful information.

Typical perpendicular-to-plane response is illustrated

in Fig. 3. In this case the current operator is diagonal in orbital, but not diagonal in subband. We therefore see a number of strong spectral features as summarized in Fig. 3a. At low carrier density, the subband splittings are not much larger than the lifetime broadening η and features associated with allowed transitions are therefore obscured in Fig. 3a. In practice, however, low-carrier density t_{2g} 2DEGs tend to have higher mobilities, and therefore smaller values of η so the situation depicted in Fig. 3a may be too pessimistic. At our medium density, a peak emerges at ~ 40 meV that is associated with an optical transition from the lowest occupied heavy mass $\{yz, zx\}$ manifold to the many unoccupied subbands of $\{yz, zx\}$ character. In Fig 3b we show the electronic structure which yields these conductivities. The $\{yz, zx\}$ transitions are prominent because these bands have a large mass in one direction and therefore a larger density-of-states than xy bands, and also because the z -direction current operator is proportional to their larger inter-layer hopping amplitudes. We have highlighted the transitions responsible for the ~ 40 meV peak with green arrows in Fig. 3b.

For high densities, we see two features at ~ 16 and ~ 100 meV. We identify the higher energy features as originating from the $\{yz, zx\}$ transitions labelled "2" in Fig. 3c. (The "1" transition energy is too small to be

clearly identified on the scale of Fig. 3c.) The calculations also reveal many small features at higher energies that we associate with transitions between the most strongly confined t_{2g} subbands and the large number of bulk-like bands due to the 60 layer simulation.¹⁴ These features would become sharper if we performed our calculations with a smaller phenomenological scattering rate η . We expect, however, that in typical systems they will yield a smooth tail in the optical response. In Fig. 3c, highly dispersive nearly 3D xy subbands can be seen with a characteristic energy width of $4t' \sim 140$ meV. These subbands are more densely spaced at the top and bottom of this manifold due to the bonding between neighboring layers. The non-zero SO coupling causes hybridization within the t_{2g} manifold that allows $\{yz, xz\}$ transitions to this xy manifold. The two dominant SO mediated transitions discussed above are at 100 meV and 240 meV. The 100 meV transition gives a small contribution to the "2" peak and is therefore obscured by $\{yz, zx\}$ to $\{yz, zx\}$ transitions. We label the "3" peak by the 240 meV transition which is not obscured by the dominant $\{yz, zx\}$ to $\{yz, zx\}$ processes.

We remark that optical spectroscopy features in conventional semiconductor 2DEGs are shifted from the subband splittings by depolarization effects.^{16,26} When electrons transition to unoccupied states, the charge distribution along the z direction is altered, which in turn alters the time-dependent electric field. Similar shifts will occur in oxide 2DEGs. The peak shift is²⁶ $2e^2nES/\epsilon$ where n is the density of the electrons involved in the transition, E is the subband splitting and S is an effective Coulomb interaction length²⁶ for the corresponding transition. In the conventional case, intersubband transition energies are small enough that ϵ can be taken to be the static dielectric constant of the host semiconductor material. In the present case many of the transitions of interest involve strongly confined t_{2g} electrons, and have frequencies larger than many of the important optical phonons. (See Fig. 3a for example). In our medium density case, the transition energy falls between optical phonon modes at around 20 and 70 meV. The effective dielectric constant in bulk SrTiO₃ in this frequency range is $\epsilon \sim 10$. If we assume 10^{14} cm^{-2} $\{yz, zx\}$ electrons are involved in the transition and that the Coulomb interaction length is ~ 1 lattice constant, we estimate that the peak shift is on the order of 190 meV. This simple estimate shows that the depolarization shifts are potentially large. Because optical phonon oscillator strengths and frequencies are likely to be substantially altered close to surfaces and interfaces, a fully quantitative theory of depolarization shifts in perovskite t_{2g} 2DEGs will be quite involved.

V. SUMMARY AND CONCLUSIONS

We report on a theoretical model study of the optical conductivity of t_{2g} 2DEGs formed at perovskite oxide

surfaces and interfaces. The detailed properties of these low-dimensional electron systems are difficult to predict theoretically because of the important role played in their properties by non-local and non-linear dielectric screening and by structural distortions and defects. This study is motivated by the potential value of spectral and sum rule information from optical characterization for verification and refinement of models of t_{2g} 2DEG properties.

We find that the in-plane optical conductivity is very strongly dominated by approximately independent Drude peak contributions coming from all bands, irrespective of their t_{2g} -orbital character and of the degree to which they are confined at the interface. Unlike the *dc* conductivity, the Drude weight, obtained by integrating the Drude peak over frequency, is independent of the unknown scattering times of the various bands. Our calculations show that measuring the Drude weight of the t_{2g} 2DEG will provide an estimate of the total 2D carrier density that is complementary to the one provided by Hall effect measurements. The in-plane conductivity will also have features associated with intersubband transitions, but these will be weak unless spin-orbit interactions hybridize t_{2g} electrons with different orbital character. In the model calculations we have performed the primary source of hybridization is atomic-like spin-orbit interactions which will normally have the strongest impact. Rashba¹³ spin-orbit interactions, which we have not specifically included, could provide a gate-tunable source of spin-orbit coupling which could enhance the value of in-plane current response measurements.

Unlike its in-plane counterpart, perpendicular-to-plane optical conductivity measurements should reveal a wealth of spectroscopic measurements. Their interpretation will however be complicated by depolarization shifts which mean that spectral features cannot be immediately identified with intersubband transition energies. Based on our study we conclude that the influence of gates, particularly the influence of back gates on ellipsometry, might be helpful in assigning features to particular transitions in the t_{2g} 2DEG. When the t_{2g} carrier density is reduced by a back gate¹⁴ it has the effect of increasing the electric field deep in the substrate, which has a particularly strong influence on the weakly-confined states which are otherwise present, sharply increasing the smallest subband splittings, decreasing the number of partially occupied subbands, and increasing spatial overlap between occupied and empty subbands. We can expect that broad tails in optical response will sharpen into discrete features which can be assigned on the basis of their spectral response to back gate voltages.

Acknowledgments

This work was supported by NSF DMR 1122603 and by the Robert A Welch Foundation Grant TBF1473.

- ¹ D.G. Schlom, L.Q. Chen, X. Pan, A. Schmehl, and M.A. Zurbuchen, *Journal of the American Ceramic Society* **91**, 2429 (2008).
- ² J. Son, P. Moetakef, B. Jalan, O. Bierwagen, N.J. Wright, R. Engel-Herbert, and S. Stemmer, *Nat Mater* **9**, 482 (2010).
- ³ A. Ohtomo and H.Y. Hwang, *Nature* **427**, 423 (2004).
- ⁴ A. Brinkman, M. Huijben, M. van Zalk, J. Huijben, U. Zeitler, J.C. Maan, W.G. van der Wiel, G. Rijnders, D.H.A. Blank, and H. Hilgenkamp, *Nature Materials* **6**, 493 (2007).
- ⁵ N. Reyren, S. Thiel, A.D. Caviglia, L. Fitting Kourkoutis, G. Hammerl, C. Richter, C.W. Schneider, T. Kopp, A.S. Ruetschi, D. Jaccard, M. Gabbay, D.A. Muller, J.M. Triscone, and J. Mannhart, *Science* **317**, 1196 (2007).
- ⁶ L. Li, C. Richter, J. Mannhart, and R.C. Ashoori, *Nature Physics* **7**, 762 (2011); D.A. Dikin, M. Mehta, C.W. Bark, C.M. Folkman, C.B. Eom, and V. Chandrasekhar, *Phys. Rev. Lett.* **107**, 056802 (2011); J.A. Bert, B. Kalisky, C. Bell, M. Kim, Y. Hikita, H.Y. Hwang, and K.A. Moler, *Nat. Phys.* **7**, 767 (2011); P. Moetakef, J.R. Williams, D.G. Ouellette, A.P. Kajdos, D. Goldhaber-Gordon, S.J. Allen, and S. Stemmer, *Phys. Rev. X* **2**, 021014 (2012).
- ⁷ J. Mannhart and D.G. Schlom, *Science* **327**, 1607 (2010); J. Mannhart, D.H.A. Blank, H.Y. Hwang, A.J. Millis, and J.-M. Triscone, *MRS Bulletin* **33**, 1027 (2008).
- ⁸ A. Ohtomo, D.A. Muller, J.L. Grazul, and H.Y. Hwang, *Nature* **419**, 378 (2002);
- ⁹ P. Moetakef, T.A. Cain, D.G. Ouellette, J.Y. Zhang, D.O. Klenov, A. Janotti, C.G. Van de Walle, S. Rajan, S.J. Allen, and S. Stemmer, *Appl. Phys. Lett.* **99**, 232116 (2011); P. Moetakef, J.Y. Zhang, A. Kozhanov, B. Jalan, R. Seshadri, S.J. Allen, and S. Stemmer, *Appl. Phys. Lett.* **98**, 112110 (2011);
- ¹⁰ K. Ueno, S. Nakamura, H. Shimotani, A. Ohtomo, N. Kimura, T. Nojima, H. Aoki, Y. Iwasa, and M. Kawasaki, *Nature Materials* **7**, 855 (2008); Y. Lee, C. Clement, J. Hellerstedt, J. Kinney, L. Kinnischtzke, X. Leng, S.D. Snyder, and A.M. Goldman *Phys. Rev. Lett.* **106**, 136809 (2011); M. Lee, J.R. Williams, S. Zhang, C.D. Frisbie, and D. Goldhaber-Gordon, *Phys. Rev. Lett.* **107**, 256601 (2011).
- ¹¹ B. Jalan, S.J. Allen, G.E. Beltz, P. Moetakef, and S. Stemmer, *Appl. Phys. Lett.* **98**, 132102 (2011).
- ¹² K. Ueno, S. Nakamura, and H. Shimotani, *Nature Nanotechnol.* **6**, 408 (2011); P.D.C. King, R. H. He, T. Eknapakul, P. Buaphet, S.K. Mo, Y. Kaneko, S. Harashima, Y. Hikita, M.S. Bahramy, C. Bell, Z. Hussain, Y. Tokura, Z.X. Shen, H.Y. Hwang, F. Baumberger, and W. Meevasana, *Phys. Rev. Lett.* **108**, 117602 (2012).
- ¹³ A.D. Caviglia, M. Gabay, S. Gariglio, N. Reyren, C. Cancellieri, and J.-M. Triscone, *Phys. Rev. Lett.* **104**, 126803 (2010); A. Fete, S. Gariglio, A.D. Caviglia, J.M. Triscone, and M. Gabay, *Phys. Rev. B* **86**, 201105(R) (2012); H. Nakamura, T. Koga, and T. Kimura, *Phys. Rev. Lett.* **108**, 206601 (2012); Z. Zhong, A. Toth, and K. Held, *Phys. Rev. B* **87**, 161102(R) (2013); G. Khalsa, B. Lee, and A.H. MacDonald, *Phys. Rev. B* **88**, 041302 (2013).
- ¹⁴ G. Khalsa and A.H. MacDonald, *Phys. Rev. B*, **86** 125121 (2012).
- ¹⁵ M. Stengel, *Phys. Rev. Lett.* **106**, 136803 (2011).
- ¹⁶ T. Ando, A.B. Fowler, and F. Stern, *Rev. Mod. Phys.* **54**, 437 (1982).
- ¹⁷ G. Harbeke, *Physica Scripta* **T29**, 135 (1989).
- ¹⁸ L.C. West and S.J. Eglash, *Appl. Phys. Lett.* **46**, 1156 (1985).
- ¹⁹ A complementary theoretical paper with a similar motivation appeared as we were preparing this paper for publication, S.Y. Park, and A.J. Millis, *Phys. Rev. B* **87**, 205145 (2013). These authors made an effort to connect more directly with ellipsometry, and in particular estimated the interaction induced shifts in intersubband transition energies. Our paper focuses more on features associated with the weak coupling between t_{2g} bands which can make optical characterization more useful, and accounts for their finite heavy-masses which often play an essential role.
- ²⁰ R. Kubo, *J. Phys. Soc. Jpn.* **12**, 570 (1957).
- ²¹ G. Mahan, *Many particle physics*, Springer 2010.
- ²² Z.Q. Liu, C.J. Li, W.M. Lu, X.H. Huang, Z. Huang, S.W. Zeng, X.P. Qiu, L.S. Huang, A. Annadi, J.S. Chen, J.M.D. Coey, T. Venkatesan, and Ariando, *Phys. Rev. X* **3**, 021010 (2013).
- ²³ Ming Xie, Guru Khalsa, and A.H. MacDonald, to be submitted.
- ²⁴ J.L.M. van Mechelen, D. van der Marel, C. Grimaldi, A.B. Kuzmenko, N.P. Armitage, N. Reyren, H. Hagemann, and I.I. Mazin, *Phys. Rev. Lett.* **100**, 226403 (2008); R. Cowley, *Phys. Rev.* **134**, A981 (1964).
- ²⁵ A. Janotti, D. Steiauf, and C.G. Van de Walle, *Phys. Rev. B* **84**, 201304 (2011); Y.J. Chang, G. Khalsa, L. Moreschini, A.L. Walter, A. Bostwick, K. Horn, A.H. MacDonald, and E. Rotenberg, *Phys. Rev. B* **87**, 115212 (2013).
- ²⁶ S.J. Allen, D.C. Tsui, and B. Vinter, *Solid State Commun.* **20**, 425 (1976).